

Continuous-time state-space unsteady aerodynamic modeling for efficient loads analysis

Werter, Noud P.M.; De Breuker, Roeland; Abdalla, Mostafa M.

DOI

[10.2514/1.J056068](https://doi.org/10.2514/1.J056068)

Publication date

2018

Document Version

Final published version

Published in

AIAA Journal: devoted to aerospace research and development

Citation (APA)

Werter, N. P. M., De Breuker, R., & Abdalla, M. M. (2018). Continuous-time state-space unsteady aerodynamic modeling for efficient loads analysis. *AIAA Journal: devoted to aerospace research and development*, 56(3), 905-916. <https://doi.org/10.2514/1.J056068>

Important note

To cite this publication, please use the final published version (if applicable). Please check the document version above.

Copyright

Other than for strictly personal use, it is not permitted to download, forward or distribute the text or part of it, without the consent of the author(s) and/or copyright holder(s), unless the work is under an open content license such as Creative Commons.

Takedown policy

Please contact us and provide details if you believe this document breaches copyrights. We will remove access to the work immediately and investigate your claim.



Continuous-Time State-Space Unsteady Aerodynamic Modeling for Efficient Loads Analysis

Noud P. M. Werter,* Roeland De Breuker,† and Mostafa M. Abdalla‡
Delft University of Technology, 2629 HS Delft, The Netherlands

DOI: 10.2514/1.J056068

The present paper proposes a continuous-time state-space formulation of the unsteady vortex lattice method, which is derived through a discretization of the governing advection equation for transport of vorticity in the wake. A continuous-time system is obtained by only discretizing the advection equation in space, while retaining the derivative with respect to time. The discretization in space is based on the discontinuous Galerkin method. The present method can be applied to any arbitrary nonuniform wake discretization and can be extended to higher-order panel methods or a nonflat wake shape. The method is extended to compressible flows by applying the Prandtl–Glauert transformation. The time-dependent terms in the small disturbance potential equation are neglected. Thus, incompressible flow solution procedures are applied with minimum modifications to unsteady compressible problems. The benefits are demonstrated by applying the model to the gust analysis of a general aircraft wing, varying the time step, and introducing a nonuniform wake discretization, resulting in a reduced model size for a given accuracy. The resulting continuous-time state-space model can be used for efficient loads analysis of general aircraft wings including the effects of compressibility and allows for easy integration with structural or flight dynamic models for efficient aero(servo)elastic analyses.

Nomenclature

A	=	area, m^2
A_{ss}	=	state matrix
a	=	speed of sound, m/s
B_{ss}	=	input matrix
b	=	half-chord, m
$b_{i,j}$	=	width of element i, j , m
C_{ss}	=	output matrix
c	=	chord, m
D_{ss}	=	feedthrough matrix
e_Γ	=	unit vector of a vortex segment
F	=	force vector, N
H	=	gust length, m
h_0	=	plunge amplitude, m
I	=	identity matrix
K	=	stiffness matrix
k	=	reduced frequency
M	=	Mach number
M	=	mass matrix
M	=	moment vector, Nm
N	=	number of elements
N	=	flux matrix
n	=	surface unit normal vector
p	=	pressure, N/m^2
S	=	surface
t	=	time, s
u	=	state-space input vector
V	=	velocity vector, m/s
w	=	test function
x	=	position vector, m
x	=	state-space state vector

x, y, z	=	coordinates, m
y	=	state-space output vector
α	=	angle of attack, deg
β	=	$\sqrt{1 - M^2}$
Γ	=	vortex strength, m^3/s
$\partial\Omega$	=	finite element boundary
ρ	=	air density, kg/m^3
ϕ	=	velocity potential, m^2/s
ψ	=	shape function
Ω	=	finite element domain
ω	=	frequency, rad/s
1	=	vector of ones

Subscripts

B	=	boundary
b	=	body
G	=	gust
G_{ref}	=	gust amplitude
NB	=	neighboring elements
NS	=	number of side of an element
TE	=	trailing edge
w	=	wake
w_0	=	first row of wake elements trailing the wing
x	=	with respect to xyz coordinate system
\bar{x}	=	with respect to $\bar{x}\bar{y}\bar{z}$ coordinate system
∞	=	freestream conditions

I. Introduction

ONE of the driving parameters in the design of aircraft has always been reducing weight to reduce the operating cost and make aircraft more efficient. As a consequence, wings have become more flexible, making aeroelasticity more important in wing design. To determine the dynamic response of an aircraft to, for example, a gust, an unsteady aerodynamic model is required to determine the dynamic loads.

There are several ways to predict the unsteady aerodynamic loads on an aircraft. Murua et al. [1] give an overview of unsteady aerodynamic modeling for loads analysis. The three most commonly used methods are two-dimensional (2-D) unsteady airfoil theory, the doublet lattice method (DLM), and the unsteady vortex lattice method (UVLM). A brief overview of each of these methods will be given in the following paragraphs. More recently, computational fluid dynamics-based methods have gained popularity for the analysis of, for example,

Received 13 February 2017; revision received 18 September 2017; accepted for publication 18 September 2017; published online 27 October 2017. Copyright © 2017 by Noud P. M. Werter, Roeland De Breuker, and Mostafa M. Abdalla. Published by the American Institute of Aeronautics and Astronautics, Inc., with permission. All requests for copying and permission to reprint should be submitted to CCC at www.copyright.com; employ the ISSN 0001-1452 (print) or 1533-385X (online) to initiate your request. See also AIAA Rights and Permissions www.aiaa.org/randp.

*Ph.D. Candidate, Faculty of Aerospace Engineering, Aerospace Structures and Computational Mechanics, Kluyverweg 1; N.P.M.Werter@tudelft.nl.

†Associate Professor, Faculty of Aerospace Engineering, Aerospace Structures and Computational Mechanics, Kluyverweg 1.

limit-cycle oscillations [2–5], flutter [6,7], gust response [8–11], and transonic shock buffet [12,13]. However, currently these methods are still computationally too costly to be applied for dynamic loads analysis during the preliminary design of aircraft.

Two-dimensional unsteady airfoil theory is generally referred to as strip theory. It uses closed-form solutions for several specific cases (i.e., impulsive flows, step gusts, harmonic oscillations, and sinusoidal gusts) to set up a state-space system to determine the unsteady aerodynamic loads. Strip theory has extensively been used for high-altitude long-endurance (HALE) aircraft modeling [14,15]. Two different methods to obtain a state-space system from the closed-form solutions are commonly used: this is known as Peters's finite-state method [16] and the indicial method of Leishman and Nguyen [17]. The main advantages of strip theory are its simplicity and that it allows for easy corrections (e.g., for stall). However, the main disadvantage of strip theory is that it is based on 2-D unsteady airfoil theory with three-dimensional (3-D) corrections, and thus, it cannot give any accurate information about the spanwise loading distribution.

The doublet lattice method, introduced by Albano and Rodden [18], is probably the most widely used method for unsteady load analysis of aircraft. One of the advantages of DLM is that compressibility is captured in the analysis. DLM assumes harmonic displacements on the natural vibration modes of the wing to determine the aerodynamic influence coefficients (AICs) for several reduced frequencies and flight conditions. The solution is converted from the frequency domain to the time domain by means of a rational function approximation (RFA). There are two well-known techniques for the RFA: Roger's approach using Padé approximants [19] and Karpel's minimum-state method [20]. The setup in the frequency domain makes the method especially suitable for flutter analysis. However, when time domain simulations are required, an incorrect selection of lag terms in the RFA can have a significant effect on the accuracy of the results. Especially when a discrete gust is modeled, the time lags resulting from the convection of the gust over the wing, which are expressed as phase shifts in the frequency domain, make the approximation of the gust response in the time domain by means of an RFA problematic. To overcome this problem, two methods were introduced: 1) dividing the aerodynamic model into several aerodynamic zones, each having their own gust input [21] and 2) the physical RFA [22], where instead of applying the RFA on the AICs in generalized coordinates, the RFA is applied to the AICs at a panel level, resulting in a gust input per aerodynamic panel such that the time lags can be modeled directly. Both methods, however, result in an increase in the number of aerodynamic states and still use harmonic aerodynamic data to predict the transient aerodynamic response. Furthermore, a wide range of reduced frequencies has to be covered to ensure accurate results.

The unsteady vortex lattice method uses a distribution of vortex rings over the mean aerodynamic surface to solve the potential flow equations. Katz and Plotkin [23] give a good overview of the implementation of UVLM. The main advantages of UVLM are that it is written in the time domain, and thus the transient aerodynamic response is computed directly, and that it allows for modeling of a free wake and can thus be used for the computation of the flow around wings undergoing large motions. Therefore, UVLM has recently become popular for the accurate analysis of HALE aircraft wings undergoing large deformations [1]. Furthermore, UVLM can be written in a discrete-time state-space system [24,25], allowing easy integration with other disciplines. More recently, this discrete-time form of the wake-shedding equation has been converted to continuous time by Stewart et al. [26], using the time step used to define the discrete-time system using a central differencing scheme, following a similar approach as Mohammadi-Amin et al. [27], who used a backward Euler scheme to obtain a continuous-time representation for a boundary element solution based on constant strength doublet panels. The main disadvantage of UVLM, however, is that it solves the Laplace equation and, therefore, does not account for the full effects of compressibility.

Within this field, the present paper proposes a novel continuous-time state-space formulation of UVLM, which, in contrast to Mohammadi-Amin et al. [27] and Stewart et al. [26], is directly derived through a discretization of the governing advection equation for

transport of vorticity in the wake by means of the discontinuous Galerkin method and not based on an underlying discrete-time discretization. In case the incompressible flow equations are solved, a continuous-time system is directly obtained by only discretizing the advection equation of wake vorticity in space, while retaining the derivative with respect to time. As a consequence, the present method can 1) be applied to a nonuniform wake discretization that takes advantage of the diminishing influence of vorticity as it is advected in the wake, 2) be extended to any arbitrary nonflat wake shape, and 3) be extended to higher-order panel methods.

The main limitation of the method, apart from being a small disturbance potential flow method, is in neglecting the time-dependent terms in the governing small disturbance potential equation. The Prandtl–Glauert transformation is applied to the present continuous-time formulation and the incompressible flow solution procedures are applied to the transformed geometry. It should be noted that, in case of a solution to the full compressible governing equation including time-dependent terms, the presence of time delays in the governing boundary integral equation requires a discretization of the governing equations in both space and time (see Morino [28]) and an equivalent continuous-time representation can only be sought through a discrete-time formulation.

Section II provides a brief explanation of potential flow theory in aerodynamics, which is used as the basis for the aerodynamic model, followed by the implementation of this potential flow theory in a novel continuous-time formulation of the unsteady vortex lattice method. The model is verified by applying it to several steady, unsteady, and compressible benchmark solutions, followed by the application of the model to the discrete gust analysis of a wing to illustrate the benefits of the present model, as discussed in Sec. III. Finally, conclusions will be drawn on the application of the model for efficient aeroelastic analysis.

II. Unsteady Aerodynamic Model

For efficient loads analysis, the unsteady aerodynamic model is based on potential flow theory implemented by means of the boundary element method. The underlying theory is presented in Sec. II.A, followed by the compressible boundary conditions in Sec. II.B. Section II.C presents a brief overview of the unsteady vortex lattice method used to illustrate the present approach. Finally, Sec. II.D presents the discretization of the advection equation for the transport of vorticity in the wake by means of the discontinuous Galerkin method, which is required to derive the continuous-time state-space formulation, as presented in Sec. II.E.

A. Potential Flow Theory

When the flow conditions around a wing correspond to very high Reynolds numbers, exhibit no strong shocks, neglect transonic effects, and are under small angles of attack, the small disturbance velocity potential can be introduced and the Prandtl–Glauert equation is obtained (see, for example, Blair [29], or Morino [28]). The Prandtl–Glauert transformation ($\bar{x} = x/\sqrt{1-M^2} = x/\beta$, $\bar{y} = y$, $\bar{z} = z$) is applied, resulting in the following governing equation:

$$\frac{\partial^2 \phi}{\partial \bar{x}^2} + \frac{\partial^2 \phi}{\partial \bar{y}^2} + \frac{\partial^2 \phi}{\partial \bar{z}^2} = \left(\frac{2M}{\alpha \sqrt{1-M^2}} \right) \frac{\partial^2 \phi}{\partial \bar{x} \partial t} + \left(\frac{1}{\alpha^2} \right) \frac{\partial^2 \phi}{\partial t^2} \quad (1)$$

where M is the Mach number, α is the speed of sound, and ϕ is the disturbance velocity potential defined as

$$\mathbf{V} = \mathbf{V}_\infty + \nabla_x \phi \quad (2)$$

where \mathbf{V} is the local velocity vector, \mathbf{V}_∞ is the freestream velocity vector, and the subscript \mathbf{x} indicates the xyz coordinate system.

In case of steady flow, the right-hand side of Eq. (1) reduces to zero and the Laplace equation is obtained such that incompressible flow solution procedures can be used to obtain the compressible flow solution. In case of compressible unsteady flow, the time-dependent terms need to be considered as well. However, for low to moderate subsonic Mach numbers, the right-hand side is relatively small and the solutions to the unsteady Prandtl–Glauert equation can be approximated

by solutions to the Laplace equation for the small disturbance velocity potential:

$$\nabla_{\tilde{x}}^2 \phi = 0 \quad (3)$$

The validity of the Laplace equation for compressible unsteady aerodynamics is thus dependent on the Mach number and the level of unsteadiness of the flow. A common measure for the level of unsteadiness in the flow is the reduced frequency k defined through

$$k = \frac{\omega b}{V_\infty} \quad (4)$$

where ω is the frequency and b is the reference half-chord. As long as either the reduced frequency or the Mach number is low to moderate, the incompressible flow solution is expected to approximate the unsteady compressible flow solution by applying the Prandtl–Glauert transformation and solving the Laplace equation. This observation is supported by numerical results shown in Sec. III.

To complete the definition of the problem, boundary conditions need to be specified. In aerodynamics of aircraft, these in general consist of a boundary condition enforcing flow tangency on the wing surface and a boundary condition that ensures that the flow disturbance vanishes at infinity:

$$(\nabla_x \phi + \mathbf{V}_\infty - \mathbf{V}_b) \cdot \mathbf{n} = 0, \quad \text{on the wing surface} \quad (5)$$

$$\lim_{|\mathbf{x}-\mathbf{x}_0| \rightarrow \infty} \nabla_x \phi = 0 \quad (6)$$

where \mathbf{n} is the surface unit normal vector, \mathbf{x}_0 is the position vector on the wing surface, \mathbf{x} is the position vector of the location of interest, and \mathbf{V}_b is the velocity of the wing surface with respect to the freestream velocity as, for example, introduced by aeroelastic deformations.

To model a lifting surface by means of potential flow theory, a wake surface trailing the wing needs to be introduced, which is a surface of discontinuity for ϕ . The transport of vorticity on this wake surface is governed by the advection equation as, for example, derived by Morino [28]:

$$\frac{\partial \Delta \phi}{\partial t} + \mathbf{V}_w \cdot \nabla \Delta \phi = 0 \quad (7)$$

where $\Delta \phi$ is the jump in velocity potential over the wake surface and \mathbf{V}_w is the local velocity on the wake surface. To find a solution to the problem, the jump in velocity potential in the wake needs to be related to the velocity potential on the wing surface. This relation can be found through the Kutta condition, which states that the flow leaves the sharp trailing edge of an airfoil smoothly and the velocity there is finite, resulting in

$$\Delta \phi_b|_{TE} = \Delta \phi_w|_{TE} \quad (8)$$

where $\Delta \phi_b$ is the potential difference on the body and $\Delta \phi_w$ is the corresponding potential difference in the wake along the same streamline.

A common assumption in aeroelasticity (see, for example, Giesing et al. [30]) is that the wake surface is rigidly connected to the wing and convected with the freestream velocity such that Eq. (7) reduces to

$$\frac{\partial \Delta \phi}{\partial t} + \mathbf{V}_\infty \cdot \nabla \Delta \phi = 0 \quad (9)$$

which is a valid assumption as long as the motions of the wing remain small with respect to the reference configuration.

B. Compressible Boundary Conditions

To investigate the effect of compressibility, the Prandtl–Glauert transformation also needs to be applied to the boundary conditions. In case of compressibility, the boundary condition at infinity still holds, however, the flow tangency condition, given by Eq. (5), is dependent upon the induced velocity $\nabla \phi$ at the wing surface and is therefore affected by the transformation. Defining the wing surface as $S(x, y, z, t) = 0$, such that the surface normal \mathbf{n} is given by $\nabla_x S$, the flow tangency condition, given by Eq. (5), can be written as

$$(\mathbf{V}_\infty - \mathbf{V}_b + \nabla_x \phi) \cdot \nabla_x S = 0 \quad (10)$$

and introducing the Prandtl–Glauert transformation

$$\left(\mathbf{V}_\infty - \mathbf{V}_b + \left[\frac{1}{\beta} \frac{\partial \phi}{\partial x}, \frac{\partial \phi}{\partial y}, \frac{\partial \phi}{\partial z} \right] \right) \cdot \nabla_x S = 0 \quad (11)$$

$$(\mathbf{V}_\infty - \mathbf{V}_b) \cdot \nabla_b S + \left[\frac{\partial \phi}{\partial x}, \frac{\partial \phi}{\partial y}, \frac{\partial \phi}{\partial z} \right] \cdot \left[\frac{1}{\beta} \frac{\partial S}{\partial x}, \frac{\partial S}{\partial y}, \frac{\partial S}{\partial z} \right] = 0 \quad (12)$$

As can be seen, the flow tangency boundary condition in the compressible flow solution can be computed using incompressible flow solution routines, as long as the Prandtl–Glauert transformation is applied to the wing geometry and the x component of the surface normal is divided by β .

C. Unsteady Vortex Lattice Method

To solve the potential flow problem, a collocation method is commonly used. In UVLM, the wing is modeled by vortex ring elements on its camber surface under a thin-wing approximation. As illustrated in Fig. 1, the camber surface of the wing, the first row of wake elements trailing the wing, and the free wake are discretized by N_b , N_{w_0} , and N_w quadrilateral elements, respectively. Note that the jump in velocity potential over the wing surface and the wake is equal to the vortex strength of the vortex ring elements (i.e., $\Delta \phi = \Gamma$).

The flow tangency condition, given by Eq. (5), is satisfied at N_b collocation points on the wing surface, resulting in the following set of N_b equations as, for example, derived by Katz and Plotkin [23]:

$$\mathbf{K}_1 \Gamma_b + \mathbf{K}_2 \Gamma_{w_0} + \mathbf{K}_3 \Gamma_w = -\mathbf{V} \cdot \mathbf{n} \quad (13)$$

where $\mathbf{V} \cdot \mathbf{n}$ represents the contribution of the freestream velocity and any motion of the wing surface and \mathbf{K}_1 , \mathbf{K}_2 , and \mathbf{K}_3 are the matrices of aerodynamic influence coefficients defining the induced velocities normal to the wing surface induced by the vorticity on the wing Γ_b in the first row of wake elements Γ_{w_0} and in the free wake Γ_w on the collocation points (i.e., $\nabla \phi \cdot \mathbf{n}$).

Under the assumption of small disturbances with respect to the mean steady flow solution, the right-hand side of Eq. (13) for a panel p on the wing surface reduces to

$$-\mathbf{V}_p \cdot \mathbf{n}_p = \underbrace{-\mathbf{V}_\infty \cdot \mathbf{n}_p}_{\text{mean steady flow}} \quad \underbrace{-\Delta \mathbf{V}_\infty \cdot \mathbf{n}_p}_{\text{freestream perturbation}} \quad \underbrace{-\mathbf{V}_\infty \cdot \Delta \mathbf{n}_p + \mathbf{V}_b \cdot \mathbf{n}_p}_{\text{motion of the wing surface}} \quad (14)$$

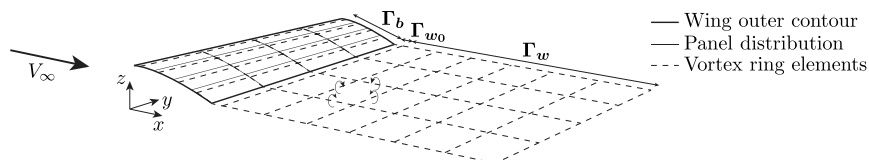


Fig. 1 Example wing discretization using vortex ring elements.

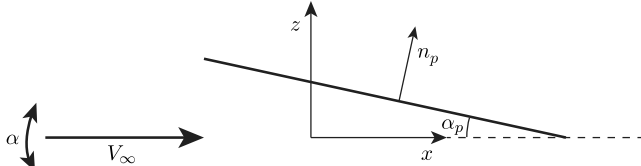


Fig. 2 Panel at an angle α_p with respect to the freestream flow.

Recognizing that the mean freestream flow V_∞ is oriented along the x axis and introducing a small perturbation angle with respect to the mean freestream flow α , as illustrated in Fig. 2, ΔV_∞ can be defined as a function of α , resulting in

$$-V_p \cdot n_p = -V_\infty n_{x_p} - V_\infty n_{z_p} \alpha - V_\infty \cdot \Delta n_p + V_b \cdot n_p \quad (15)$$

Note that, in this case, the perturbation angle α is defined by a rotation about the y axis. The same principle can, however, be extended to any arbitrary rotation in three dimensions, as long as the axis of rotation of interest for the perturbation angle α is defined beforehand. For instance, in this example, this is the y -axis or in case of wings with dihedral it will be the projection of the spanwise reference axis on the plane normal to the undisturbed flow. As a consequence, the influence of aeroelastic deformations can also be introduced by a perturbation angle of attack α similar to the definition of downwash in the doublet lattice method as, for example, given by Giesing et al. [30].

The first term in Eq. (15) represents the steady boundary condition, which is independent of time for a wing that is flying at a constant freestream velocity V_∞ with a fully developed wake. Consequently, a solution can be found by splitting the problem into two subproblems. First, a steady solution satisfying the first term in Eq. (15) is obtained, assuming constant vorticity in the wake. Second, an unsteady solution satisfying the remaining terms in Eq. (15) is obtained by developing the wake vorticity in time. Finally, by the principle of superposition, the total aerodynamic forces and moments can be found.

Next, using Eq. (8), a set of N_{w_0} equations representing the Kutta condition can be derived, resulting in

$$\mathbf{K}_4 \Gamma_b + \mathbf{K}_5 \Gamma_{w_0} = \mathbf{0} \quad (16)$$

where \mathbf{K}_4 and \mathbf{K}_5 are matrices containing ones and zeros to link each trailing-edge panel to its corresponding wake panel.

When discretizing the wake, special care needs to be taken for the panels directly trailing the trailing edge. From a physical point of view, this can be interpreted by looking at the starting vortex. When the wing is accelerated from rest and the vortex strength in the wake is still zero, the closing vortex of the first wake panel can be interpreted as the starting vortex that develops and is a lumped representation of the continuous vortex sheet shed during the initial movement of the wing. As argued by Katz and Plotkin [23], this vortex should be placed around 0.2–0.3 of the distance covered by the following wake panel.

Once the vortex strength distribution has been found, the aerodynamic forces and moments can be determined directly from the vortex strength of the vortex segments using the Kutta–Joukowski theorem, equivalent to the forces originating from the horseshoe vortices in the unsteady lifting line theory [31]. The computation of the aerodynamic forces and moments can be split into a steady component and an unsteady component, similar to Simpson et al. [32].

The steady component of the aerodynamic forces is given by the steady component of the Kutta–Joukowski theorem and is computed for each of the vortices on the wing surface under the assumption of small perturbations with respect to the freestream flow:

$$\mathbf{F}_{st} = \rho V_\infty \times \Gamma = \rho V_\infty \times e_\Gamma \Gamma \quad (17)$$

where e_Γ is the vector defining the vortex segment and Γ is the vortex strength of the vortex segment. The resulting force acts at the midpoint of the vortex segment.

The unsteady component is computed per panel according to the unsteady component of the Kutta–Joukowski theorem:

$$\mathbf{F}_{unst_i} = \rho \hat{V}_\infty \times \hat{e}_\Gamma \dot{\Gamma} A \quad (18)$$

where \hat{V}_∞ is the unit vector in the direction of the freestream flow velocity, \hat{e}_Γ is the unit vector in the direction of the leading vortex segment of the panel, A is the surface area of the panel, and the dot indicates a time derivative. Finally, the aerodynamic moments can be computed by defining a set of reference axes with respect to which the aerodynamic moments are computed.

Using Eqs. (17) and (18) for the steady and unsteady forces, the total aerodynamic forces and moments can be related to the vortex strength according to

$$\begin{bmatrix} \mathbf{F} \\ \mathbf{M} \end{bmatrix} = \begin{bmatrix} \mathbf{F}_{st} \\ \mathbf{M}_{st} \end{bmatrix} + \begin{bmatrix} \mathbf{F}_{unst} \\ \mathbf{M}_{unst} \end{bmatrix} = \mathbf{L}_1 \Gamma_b + \mathbf{L}_2 \dot{\Gamma}_b \quad (19)$$

where \mathbf{L}_1 represents the contribution of the steady component of the Kutta–Joukowski theorem and \mathbf{L}_2 represents the contribution of the unsteady component of the Kutta–Joukowski theorem.

Now that the flow tangency condition, Kutta condition, and computation of aerodynamic forces and moments have been discretized, only the discretization of transport of vorticity in the wake [Eq. (9)] is left to obtain the complete unsteady aerodynamic model. This is presented in the next section.

D. Transport of Vorticity in the Wake

Once the vortex strength at the start of the wake is known, the transport of vorticity in the wake is governed by the advection equation, given by Eq. (7). To solve Eq. (7), the discontinuous Galerkin method, as introduced by Reed and Hill [33] and discussed in more detail by Li [34], is used. The wake is discretized using finite elements that geometrically coincide with wake panels and the solution $\Delta\phi$ is approximated by an interpolation function $\Delta\phi_h$, which is continuous within each element, but generally discontinuous across element boundaries.

First, Eq. (7) is multiplied with a test function w_h integrated by parts over each element individually and then summed over all elements to obtain the weak formulation:

$$\sum_{k=1}^{N_w} \left(\int_{\Omega_k} w_h \frac{\partial \Delta\phi_h}{\partial t} - V_\infty \cdot \nabla w_h \Delta\phi_h dV + \int_{\partial\Omega_k} w_h \Delta\phi_h V_\infty \cdot \mathbf{n}_k dS \right) = 0 \quad (20)$$

where k is the element index, Ω_k represents the surface of element k , $\partial\Omega_k$ represents the boundary of element k , and \mathbf{n}_k is the outward unit normal on the element boundary.

Next, the flux of vorticity along the boundary of each element (i.e., $\Delta\phi_h V_\infty$) is approximated by a numerical flux as a function of the interpolation function $\Delta\phi_h$ on each side of the boundary, as illustrated in Fig. 3. The numerical flux is typically defined as a function of the mean and jump of, in this case, $\Delta\phi$ across the boundary, defined by

$$\overline{\Delta\phi_h} = \frac{1}{2} (\Delta\phi_h^+ + \Delta\phi_h^-); \quad [\Delta\phi_h] = \Delta\phi_h^+ \mathbf{n}^+ + \Delta\phi_h^- \mathbf{n}^- \quad (21)$$

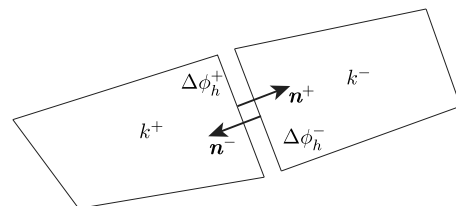


Fig. 3 Definition of the numerical flux between element k (k^+) and its neighboring element k^- .

resulting in a numerical flux of

$$\Delta\phi_h V_\infty = V_\infty \overline{\Delta\phi_h} + C_V \cdot [\Delta\phi_h] \quad (22)$$

where C_V is a nonnegative definite matrix dependent on the value of $V_\infty \cdot \mathbf{n}$.

Next, $\Delta\phi_h$ and w_h are defined by an expansion using a set of p (orthogonal) basis functions ψ on each element k :

$$\Delta\phi_h = \sum_{k=1}^{N_w} \sum_{m=1}^p \Delta\hat{\phi}_{k,m}(t) \psi_{k,m}(\mathbf{x}) \quad (23)$$

$$w_h = \sum_{k=1}^{N_w} \sum_{m=1}^p \hat{w}_{k,m} \psi_{k,m}(\mathbf{x}) \quad (24)$$

where the coefficients $\hat{w}_{k,m}$ can be chosen arbitrarily and $\Delta\hat{\phi}_{k,m}$ are unknown functions of time. A convenient choice for the coefficients $\hat{w}_{k,m}$ is to set one coefficient equal to one, while setting all other coefficients equal to zero. Following this approach, a set of p ordinary differential equations can be derived for the unknown coefficients $\Delta\hat{\phi}$ for each element k as, for example, shown by Li [34]:

$$\mathbf{M} \frac{\partial \Delta\hat{\phi}_k}{\partial t} + \left(\mathbf{K} + \sum_{i=1}^{NS} \mathbf{K}_{B,i} \right) \Delta\hat{\phi}_k + \sum_{i=1}^{NS} N_{B,i} \Delta\hat{\phi}_{(NB,i)} = 0 \quad (25)$$

where the mass matrix \mathbf{M} and the stiffness matrix \mathbf{K} are defined by the integral in Eq. (20), $\mathbf{K}_{B,i}$ and $N_{B,i}$ represent the contribution of the numerical flux defined by Eq. (22) across the boundary of the element, $\Delta\hat{\phi}_k$ are the degrees of freedom of element k , $\Delta\hat{\phi}_{(NB,i)}$ are the degrees of freedom of the neighboring elements, and NS is the number of sides along the boundary of the element.

In our implementation, a classical upwinding scheme given by $C_V = 1/2(V_\infty \cdot \mathbf{n})\mathbf{I}$ and piecewise constant basis functions [i.e., $\psi_{k,m}(\mathbf{x}) = 1$] have been selected, such that each wake element can be represented by an equivalent vortex ring element with strength $\Gamma_k(t) = \Delta\phi_k(t)$. Recognizing that, as illustrated in Fig. 1, V_∞ is oriented along the x axis and always positive such that vorticity is transported in the positive x direction, the element equation [Eq. (25)] reduces to

$$A_{i,j} \dot{\Gamma}_{w_{i,j}} + (\Gamma_{w_{i,j-1}}(t) - \Gamma_{w_{i,j}}(t)) V_\infty b_{i,j} = 0 \quad (26)$$

$$\dot{\Gamma}_{w_{i,j}} = \frac{(\Gamma_{w_{i,j}}(t) - \Gamma_{w_{i,j-1}}(t)) V_\infty}{\Delta x_{w_{i,j}}} \quad (27)$$

where $A_{i,j}$ is the area of the element, $b_{i,j}$ is the width of the element perpendicular to the flow direction, Δx_w is the wake panel length in the flow direction, and the element number k has been replaced by a spanwise element index i and a streamwise element index j to reflect the transport of vorticity in the streamwise direction.

Finally, by assembling all element equations, the transport of vorticity in the wake is governed by the following matrix equation:

$$\dot{\Gamma}_w = \mathbf{K}_6 \Gamma_w + \mathbf{K}_7 \Gamma_{w_0} \quad (28)$$

where \mathbf{K}_6 represents the transport of vorticity throughout the wake and \mathbf{K}_7 introduces the influx of vorticity in the wake governed by the first row of wake elements.

Note that Eq. (7) has only been discretized in space and no assumptions are made regarding the time derivative. As a consequence, this approach allows for implementation of arbitrary wake shapes, wake discretizations (structured and nonstructured), or higher-order panel methods, while retaining a continuous-time representation. As long as the jump in velocity potential at the trailing edge is known, Eq. (7) and the discontinuous Galerkin method can be used to describe and discretize the transport of vorticity in the wake, after which the

choice of singularity element will determine the final set of discretized equations. Instead of a wake that is aligned with the undisturbed freestream flow, the present approach can, for example, also be applied to a prescribed wake geometry including the effects of wake roll up as, for example, used by Murua et al. [1] and Hesse and Palacios [35] in their discrete-time formulation. Furthermore, besides introducing a nonuniform wake discretization, as presented in Sec. II.C, that takes advantage of the diminishing influence of vorticity as it is advected in the wake, possible future improvements in efficiency can be made by reducing the computational effort required for the wake by converting wake elements downstream of the wing to vortex particles, as introduced by Voutsinas [36] or Willis et al. [37].

E. Continuous-Time State-Space Formulation

The system of equations, given by Eqs. (13), (16), and (28), can now be assembled in a continuous-time state-space form, following the derivation of Mohammadi-Amin et al. [27], however, in this case, generalized to any generic wing shape and applicable to any arbitrary wake shape or discretization. The resulting governing equation, as derived in Appendix A, is given by

$$\dot{\Gamma}_w = \mathbf{K}_8 \Gamma_w + \mathbf{K}_9 \alpha + \mathbf{K}_{10} \quad (29)$$

where α is the perturbation angle of attack on the wing surface, \mathbf{K}_8 represents the contribution of the wing and wake, \mathbf{K}_9 represents the contribution of perturbing the freestream flow, and \mathbf{K}_{10} represents the contribution of the motion of the wing surface.

Similarly, the aerodynamic forces and moments can also be related to the vortex strength of the free wake panels, the perturbation angle of attack on the wing surface, and the motion of the wing surface, as derived in Appendix B, resulting in

$$\begin{bmatrix} \mathbf{F} \\ \mathbf{M} \end{bmatrix} = \mathbf{L}_9 \Gamma_w + \mathbf{L}_{10} \alpha + \mathbf{L}_7 \dot{\alpha} + \mathbf{L}_{11} \quad (30)$$

where \mathbf{L}_9 represents the contribution of the wing and wake, \mathbf{L}_7 and \mathbf{L}_{10} represent the contribution of perturbing the freestream flow, and \mathbf{L}_{11} represents the contribution of the motion of the wing surface.

Identifying $[\dot{\alpha}, \mathbf{I}]^T$ as state-space input \mathbf{u} , $[\Gamma_w, \alpha]^T$ as state vector \mathbf{x} , and $[\mathbf{F}, \mathbf{M}]^T$ as output vector \mathbf{y} , a standard continuous-time state-space system is obtained:

$$\dot{\mathbf{x}} = \underbrace{\begin{bmatrix} \mathbf{K}_8 & \mathbf{K}_9 \\ 0 & 0 \end{bmatrix}}_{\mathbf{A}_{ss}} \mathbf{x} + \underbrace{\begin{bmatrix} 0 & \mathbf{K}_{10} \\ \mathbf{I} & 0 \end{bmatrix}}_{\mathbf{B}_{ss}} \mathbf{u} \quad (31)$$

$$\mathbf{y} = \underbrace{\begin{bmatrix} \mathbf{L}_9 & \mathbf{L}_{10} \end{bmatrix}}_{\mathbf{C}_{ss}} \mathbf{x} + \underbrace{\begin{bmatrix} \mathbf{L}_7 & \mathbf{L}_{11} \end{bmatrix}}_{\mathbf{D}_{ss}} \mathbf{u} \quad (32)$$

where \mathbf{I} is a vector of ones in all components and \mathbf{I} is the identity matrix. Note that a unique input can be specified for each wing panel, allowing for any arbitrary chordwise and spanwise gust distribution to be modeled.

The continuous-time state-space formulation can, for example, be used to find the unsteady aerodynamic response of a wing to a discrete “1 – cos” gust, as defined by

$$V_G^i(t) = \begin{cases} \frac{1}{2} V_{G,\text{ref}} \left(1 - \cos \left(\frac{2\pi V_\infty (t-t_0^i)}{H} \right) \right) & \text{for } 0 \leq t - t_0^i \leq \frac{H}{V_\infty} \\ 0 & \text{otherwise} \end{cases} \quad (33)$$

where V_G is the gust velocity at location \mathbf{x}_i , $V_{G,\text{ref}}$ is the vertical gust velocity amplitude, t_0^i is the time at which the gust reaches location \mathbf{x}_i , and H is the gust length. The corresponding input to the state-space equations can be found by converting the gust velocity to an equivalent gust angle (i.e., $\alpha_G^i = V_G^i/V_\infty$) and taking the time derivative, resulting in

$$\alpha_G^i(t) = \begin{cases} \frac{1}{2} \frac{V_{G_{ref}}}{V_\infty} \left(1 - \cos\left(\frac{2\pi V_\infty (t-t_0^i)}{H}\right) \right) & \text{for } 0 \leq t - t_0^i \leq \frac{H}{V_\infty} \\ 0 & \text{otherwise} \end{cases} \quad (34)$$

where α_G^i is the angle of attack induced by the gust velocity on the collocation point of panel i , located at \mathbf{x}_i .

Finally, the unsteady aerodynamic response can be found by any standard state-space solver, where it is important to note that, in contrast to a discrete-time formulation where the stability of the explicit time marching scheme limits the maximum time step [Courant–Friedrichs–Lewy (CFL) condition: $CFL \leq 1$], no assumptions regarding a time integration scheme have been made in the present model and, consequently, depending on the stability of the time integration scheme chosen, larger time steps can be used ($CFL > 1$).

In conclusion, under the assumption of small perturbations of a thin wing around a steady-state reference configuration, the inviscid, (in)compressible, irrotational, unsteady aerodynamic forces and moments acting on any generic wing are computed using a continuous-time state-space model, allowing for easy integration with structural or flight dynamic models for efficient aero(servo) elastic analysis using any arbitrary wake shape and discretization and a time step solely governed by accuracy requirements. The input vector allows for a unique time-dependent input for each panel on the wing surface, allowing for any arbitrary chordwise and spanwise gust distribution to be modeled. Once the unsteady aerodynamic response has been found, the total aerodynamic response can be found by the principle of superposition of the steady and unsteady aerodynamic solution.

III. Results

First, the state-space unsteady aerodynamic model, as described in Sec. II, is assessed in Sec. III.A by running the model for different unsteady benchmark cases and comparing the results to the literature. The effect of Mach number and reduced frequency on the compressible flow solution is discussed in Sec. III.B. Finally, a gust analysis study is carried out to illustrate the advantages of the current model. For all results presented, first a mesh convergence study has been carried out.

A. Verification

To verify the unsteady aerodynamic response, the unsteady aerodynamic model is first compared with 2-D unsteady results in the literature by modeling a wing with an aspect ratio of 200. To do a fair comparison to the 2-D results, the results from the literature have been compared with the section lift coefficient at the center of the wing.

Figures 4a and 4b show the comparison of the present model to the lift and moment coefficient as predicted by Theodorsen [38] for the harmonic pitch, plunge oscillation of a 2-D flat plate at different reduced frequencies. The flat plate pitches around the quarter-chord axis with an amplitude of 1 deg, has a plunge amplitude of $h_0/b = 0.02/k$, and has been investigated for $k = 0.1$, $k = 0.4$, $k = 1.0$, and $k = 3.0$. The wing is discretized using 8 spanwise and 32 chordwise elements. The wake is truncated at 20 times the chord and the wake is discretized according to $\Delta x_w/c = 1/32$. As can be seen, the present model shows excellent agreement for $k = 0.1$ and $k = 0.4$. As the reduced frequency increases, the present model overpredicts the lift and moment coefficient, which can be explained by the fact that, for the present model, the wake needs to be discretized, whereas Theodorsen computes the lift and moment coefficient analytically. Especially at higher reduced frequencies, the effect of this discretization becomes more pronounced because the number of wake panels traveled per oscillation becomes smaller. It should be noted, however, that, for most practical applications, a reduced frequency of 0.4 is already high.

Aircraft in general have a combination of taper, sweep, dihedral, twist, and camber. However, to the authors' knowledge, no results are available in literature on the unsteady aerodynamic response of panel methods for thin general aircraft wings. Therefore, to verify the 3-D unsteady aerodynamic response, the present model is compared with the unsteady aerodynamic response for rectangular wings. Figure 5a shows the comparison of the present model to the sudden acceleration of a flat rectangular wing with an aspect ratio of 6 to the results obtained by Jones [39]. The wing is discretized using 8 spanwise and 32 chordwise elements. The wake is truncated at 10 times the chord and the wake is discretized according to $\Delta x_w/c = 1/32$. As was shown by Katz for UVLM [40], because the present model can only represent a finite acceleration rate due to its wake discretization, whereas the solution by Jones [39] accounts for the infinite acceleration rate, a moderately higher initial lift can be expected for

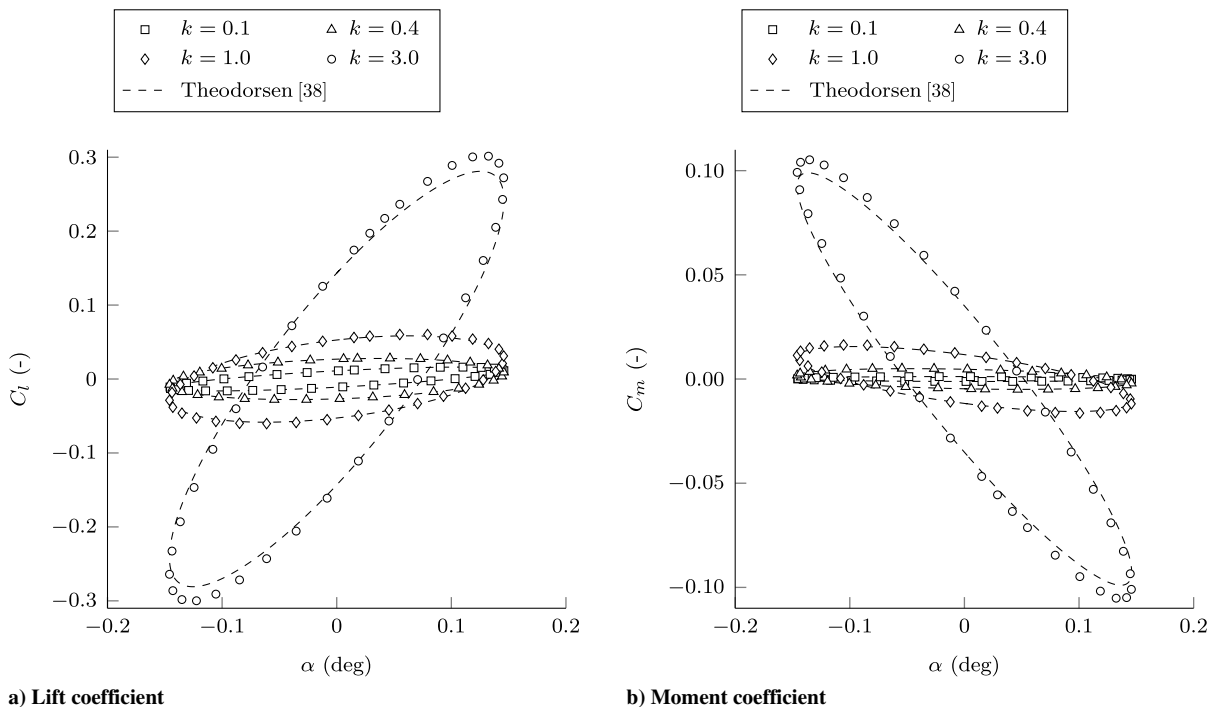
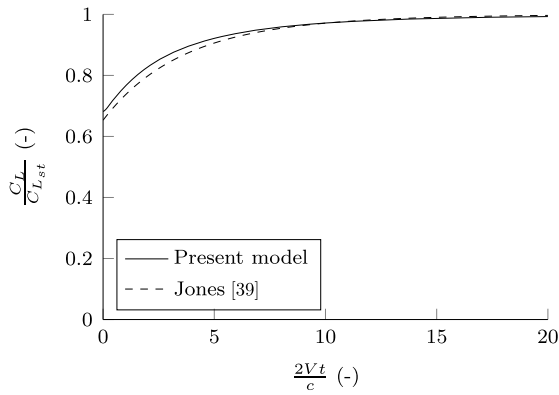
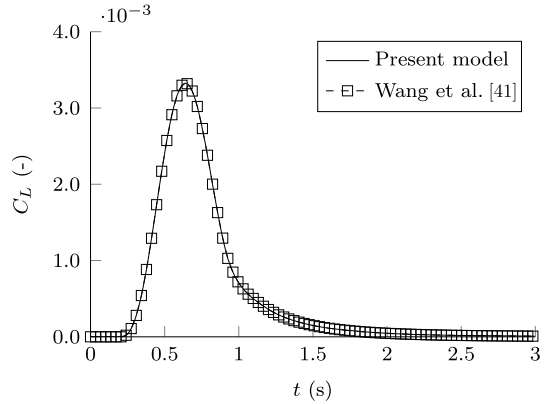


Fig. 4 Verification using a 2-D flat plate undergoing a harmonic pitch, plunge oscillation



a) Sudden acceleration of a rectangular wing with an aspect ratio of 6



b) Gust response of the Golland wing undergoing a 1-cosine gust

Fig. 5 Verification of the 3-D unsteady aerodynamic results

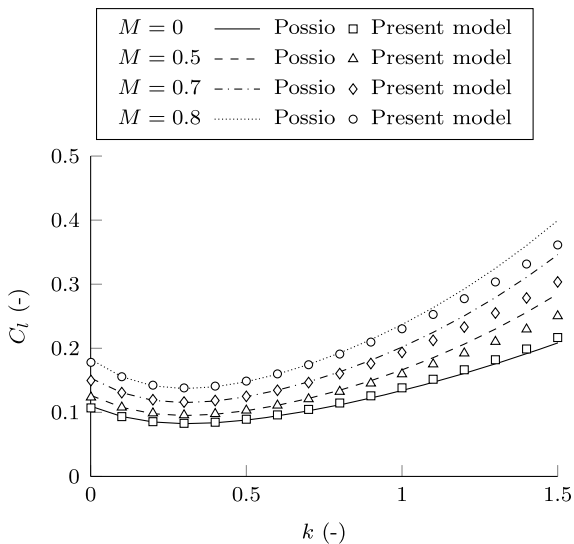
the present model, after which the solution converges to the solution by Jones.

As a final verification for the unsteady aerodynamic response, the present model is compared with the results obtained by Wang et al. [41] using UVLM for the gust response of the Golland wing under a $1 - \cos$ gust. The wing is discretized using 8 spanwise and 32 chordwise elements. The wake is truncated at 10 times the chord and the wake is discretized according to $\Delta x_w/c = 1/32$. As can be seen in Fig. 5b, the results show excellent agreement.

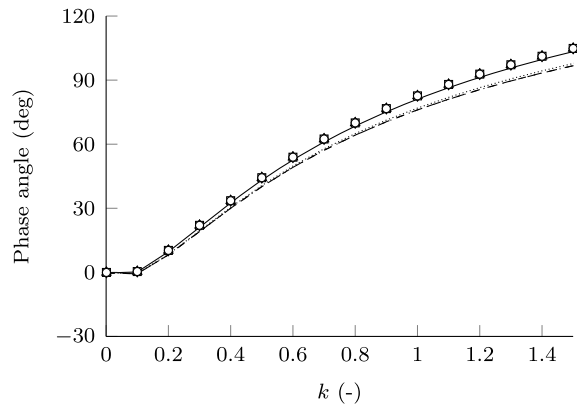
In conclusion, the present model shows excellent agreement with results in the literature for the unsteady aerodynamic response of wings, thus verifying the present model.

B. Compressible Flow

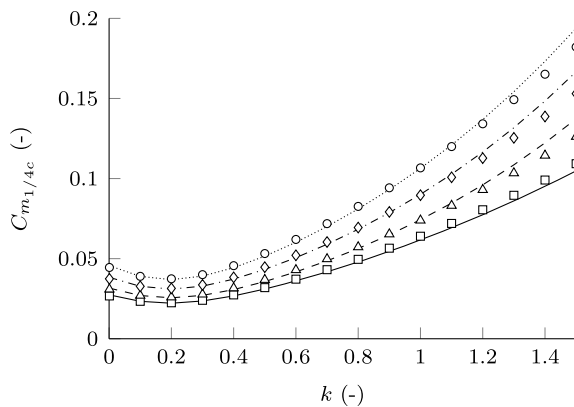
To investigate the effect of reduced frequency and Mach number on the validity of the present model for unsteady compressible flow, the present model is compared with the approximate closed-form solution, derived by Lin and Iliff [42], for the Possio integral



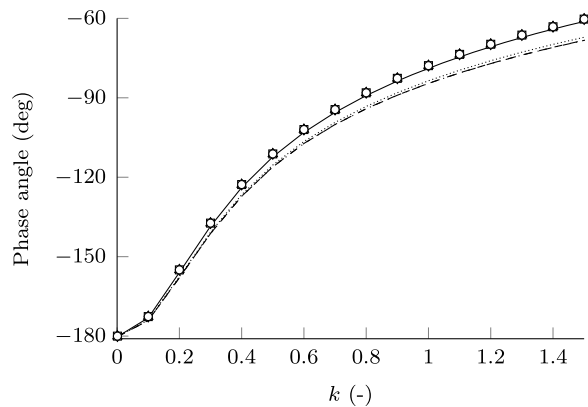
a) Lift coefficient amplitude



b) Phase angle of the lift coefficient



c) Moment coefficient amplitude



d) Phase angle of the moment coefficient

Fig. 6 Comparison with the closed-form solution [42] for a pitching thin 2-D airfoil.

Table 1 Wing properties

Property	Value
Semispan	5.0 m
Root chord	1.0 m
Taper ratio	0.3
1/4c sweep angle	30 deg
Dihedral angle	5 deg
Camber	0%
Mean aerodynamic chord	0.713 m

Table 2 Maximum lift and moment coefficient for different gust lengths.

Gust length	$C_{L_{\max}}$	$C_{M_{1/4c, \max}}$
5c	0.133	-0.262
10c	0.197	-0.358
20c	0.232	-0.410
50c	0.250	-0.438
Steady	0.256	-0.451

equation, describing the pressure distribution of a lifting surface in two-dimensional, oscillatory, subsonic compressible flow. The wing is discretized using 12 spanwise and 32 chordwise elements. The wake is truncated at 20 times the chord and the wake is discretized according to a constant wake element size of $\Delta x_w/c = 1/32$.

The resulting comparison in amplitude and phase for both lift coefficient and moment coefficient of an airfoil pitching with an amplitude of 1 deg about the quarter-chord is shown in Fig. 6 for different reduced frequencies and Mach numbers. As can be concluded from Figs. 6a and 6c, the present model shows excellent agreement to the closed-form solution in amplitude up to a reduced frequency of one, after which the effects of compressibility are no longer captured by the present model. Regarding the phase angle, as expected, the present model results in a phase angle independent of Mach number, whereas the unsteady terms in the Prandtl–Glauert equation introduce a change in phase angle resulting from the effects of compressibility. However, at a Mach number of 0.8 and a reduced frequency of one, the error in phase is still less than 10 deg.

Based on these results, it can be concluded that, as expected, with increasing reduced frequency and Mach number, the unsteady terms in the Prandtl–Glauert equation are no longer negligible and the present model can no longer capture the full effects of compressibility on the unsteady aerodynamic solution. However, although care should be taken, the results show that the present model provides sufficiently accurate dynamic load predictions at low to moderate Mach numbers and reduced frequencies encountered in the normal operating conditions of aircraft. Note, however, that at Mach numbers above 0.7 care should be taken in applying both the present model and the closed-form solution, because, depending on the wing geometry, the underlying assumptions of the linearized potential flow equations might no longer be valid and, for example, solutions to the Euler equations might be necessary for accurate results.

C. Gust Response

Finally, the model is applied to the analysis of a swept, tapered wing with the properties given in Table 1 under a $1 - \cos$ gust of various lengths, as defined by Eq. (33), to illustrate the advantages of the present continuous-time state-space model. The freestream velocity is set to 100 m/s at sea level. The gust lengths considered

are 5, 10, 20, and 50 times the mean aerodynamic chord, equivalent to a reduced frequency of 0.628, 0.314, 0.157, and 0.063, respectively. The gust amplitude is 5.24 m/s, such that the induced gust angle of attack is 3 deg. The number of spanwise and chordwise vortex ring elements is kept constant at 16 and the wake is truncated at 20 chords behind the wing. Two sets of analyses are run: 1) with constant size wake elements, while the wake discretization is varied between $\Delta x_w/c = 1/2$ and $\Delta x_w/c = 1/32$ and 2) with increasing wake element size aft of the wing. The first set of analyses has been run to provide a direct comparison to discrete-time simulations, whereas the second set has been run to illustrate the possibility to improve the efficiency of the model by varying the wake element size. An additional analysis with a constant wake discretization of $\Delta x_w/c = 64$ is used as the converged reference solution. The resulting lift and moment coefficients for different gust lengths, at the finest constant size wake discretization, are shown in Fig. 7. The corresponding maximum lift and moment coefficients are given in Table 2.

To investigate the effect of time step and wake discretization on the accuracy of the results at different reduced frequencies, the remainder of this section will only focus on gust lengths of 5 chords (i.e., highly unsteady) and 50 chords (i.e., quasi steady). Similar conclusions can be drawn for other gust lengths. Note that, in case of discrete-time state-space systems, the wake discretization and time step size are inherently linked and cannot be varied independently, unlike the present model, highlighting one of the advantages of the present approach.

Figure 8 shows the effect of a varying time step on the maximum lift and moment coefficient for different wake discretizations. Note that, in this case, all simulations were run with a constant time step size; however, in contrast to discrete-time state-space systems, the continuous-time formulation of the present model also allows for an adaptive time step to be used in the time integration, as required. The equivalent discrete-time state-space results, where the time step matches the wake discretization, are designated by the filled markers.

Several conclusions can be drawn on the effect of wake discretization and time step on the accuracy of the results. First of all, as can be expected, the results for a gust length of 50 chords converge faster than the results for a gust length of 5 chords, because a shorter

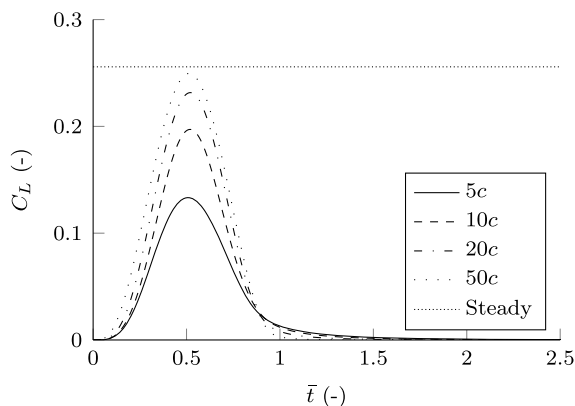
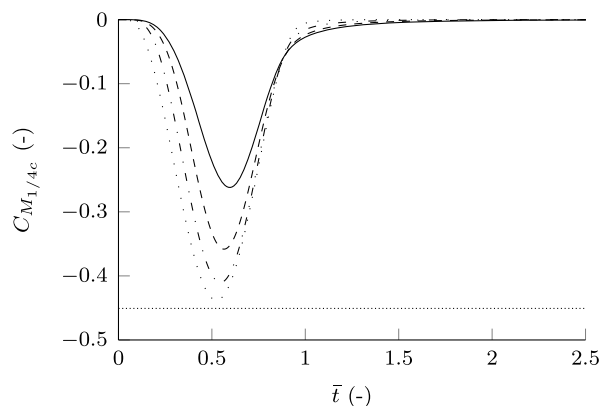
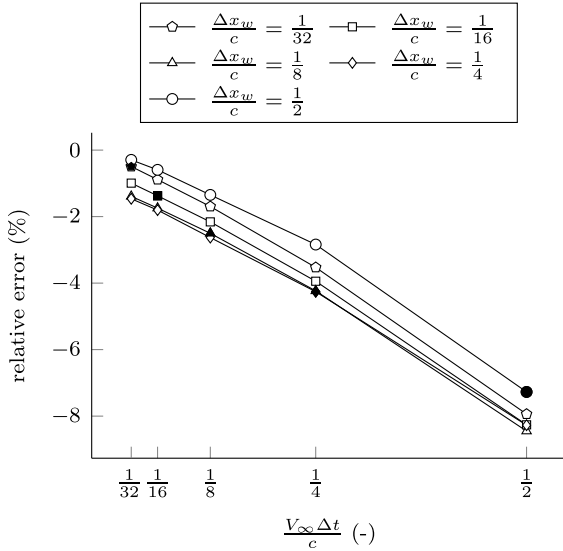
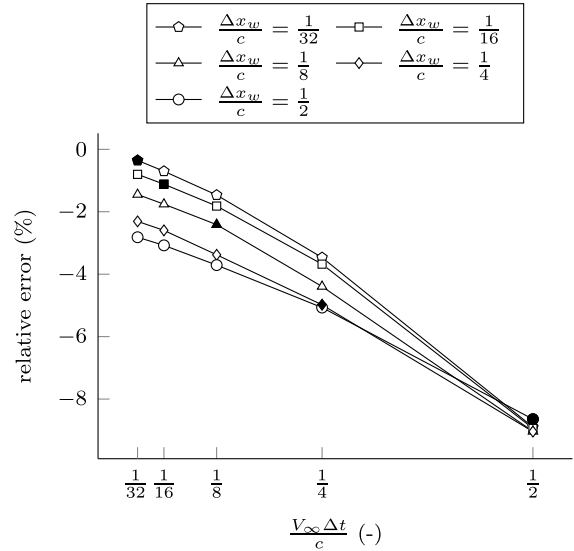
a) C_L of a 1-cosine gust of different lengthsb) $C_{M_{1/4c}}$ of a 1-cosine gust of different lengths

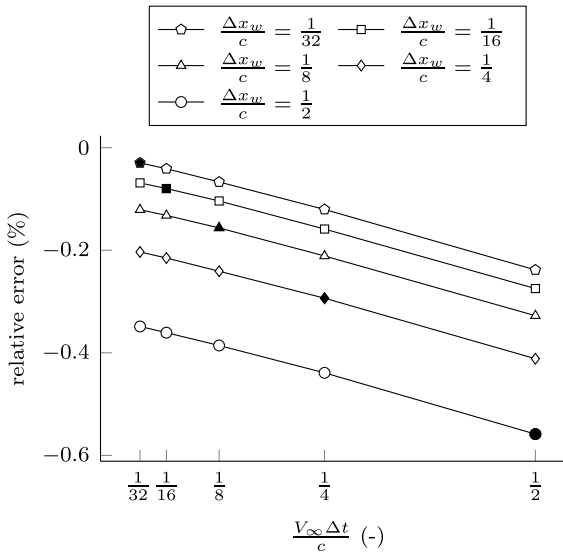
Fig. 7 Effect of gust length on the unsteady aerodynamic response. Time is normalized with respect to the time required for the gust to traverse the wing.



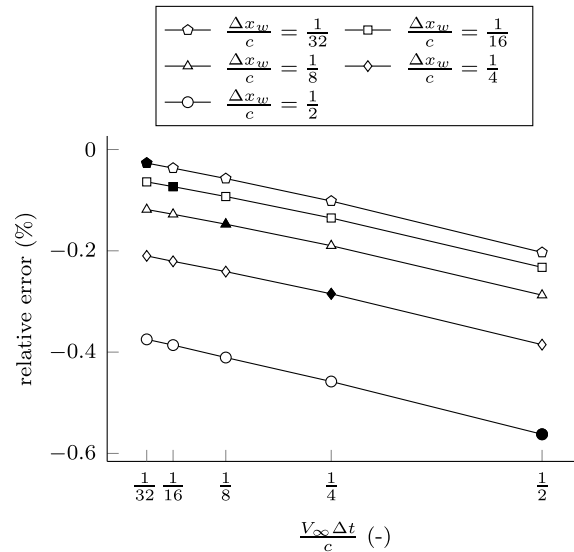
a) Relative error in maximum lift coefficient, $H = 5c$



b) Relative error in maximum moment coefficient, $H = 5c$



c) Relative error in maximum lift coefficient, $H = 50c$



d) Relative error in maximum moment coefficient, $H = 50c$

Fig. 8 Varying the time step for time integration for various wake discretizations. Equivalent discrete-time results are indicated by filled markers. The solution with a constant wake element size of $\Delta x_w/c = 1/64$ and corresponding time step of $V_\infty \Delta t/c = 1/64$ has been used as reference solution.

gust length implies a higher reduced frequency, and therefore, finer wake and time discretizations are required to obtain accurate results.

Second of all, the results clearly show the advantage of the present model, for example, for a gust length of 5 chords, a wake discretization of 8 panels per chord and the equivalent time step of $V_\infty \Delta t/c = 1/8$ results in an error of 2.5%, whereas a wake discretization of only 4 panels per chord with a smaller time step of $V_\infty \Delta t/c = 1/16$ only results in an error of 1.8%, thus clearly showing the advantage of the variable time step.

Finally, it is interesting to note that, for the lift coefficient at a gust length of 5 chords, the best result is achieved with a wake discretization of only 2 panels per chord and a time step of $V_\infty \Delta t/c = 1/32$. However, care should be taken, because depending on the gust length, both the convergence rate and the direction of convergence change. This can be explained by a combination of effects: 1) Depending on the gust length, the resulting aerodynamic forces are dominated by steady or unsteady effects, and thus, by the vorticity distribution in the wake or the time rate of change of the vorticity distribution in the wake. 2) As the wake is refined, the vorticity distribution in the wake is captured more accurately and, depending on the vorticity distribution and its time rate of change, as the discretization is improved, the resulting lift

and moment coefficient might increase or decrease. In case of a wake discretization of only 2 panels per chord, the combination of these effects results in a lift coefficient that is very close to the converged solution; however, as can be seen in Fig. 8b, the error in moment coefficient is still 2.8%, indicating a nonconverged solution.

Figure 9 shows the effect of a nonconstant wake discretization on the maximum lift and moment coefficient for different sizes of the first wake panel $\Delta x_w/c$, for a constant converged time step of $V_\infty \Delta t/c = 1/32$. The number of streamwise wake panels is reduced from a constant wake to 1/16th of the number of streamwise wake panels in a constant wake, while maintaining the size of the first wake panel and increasing the element size of the remaining wake elements as the distance behind the wing increases. The ratio in size between two adjacent elements is kept constant through the following relation, which maps a uniform element distribution ρ ($0 \leq \rho \leq 1$) onto a nonuniform element distribution r ($0 \leq r \leq 1$), as given by Weatherill et al. [43]:

$$r = \frac{e^{A\rho} - 1}{e^A - 1} \quad (35)$$

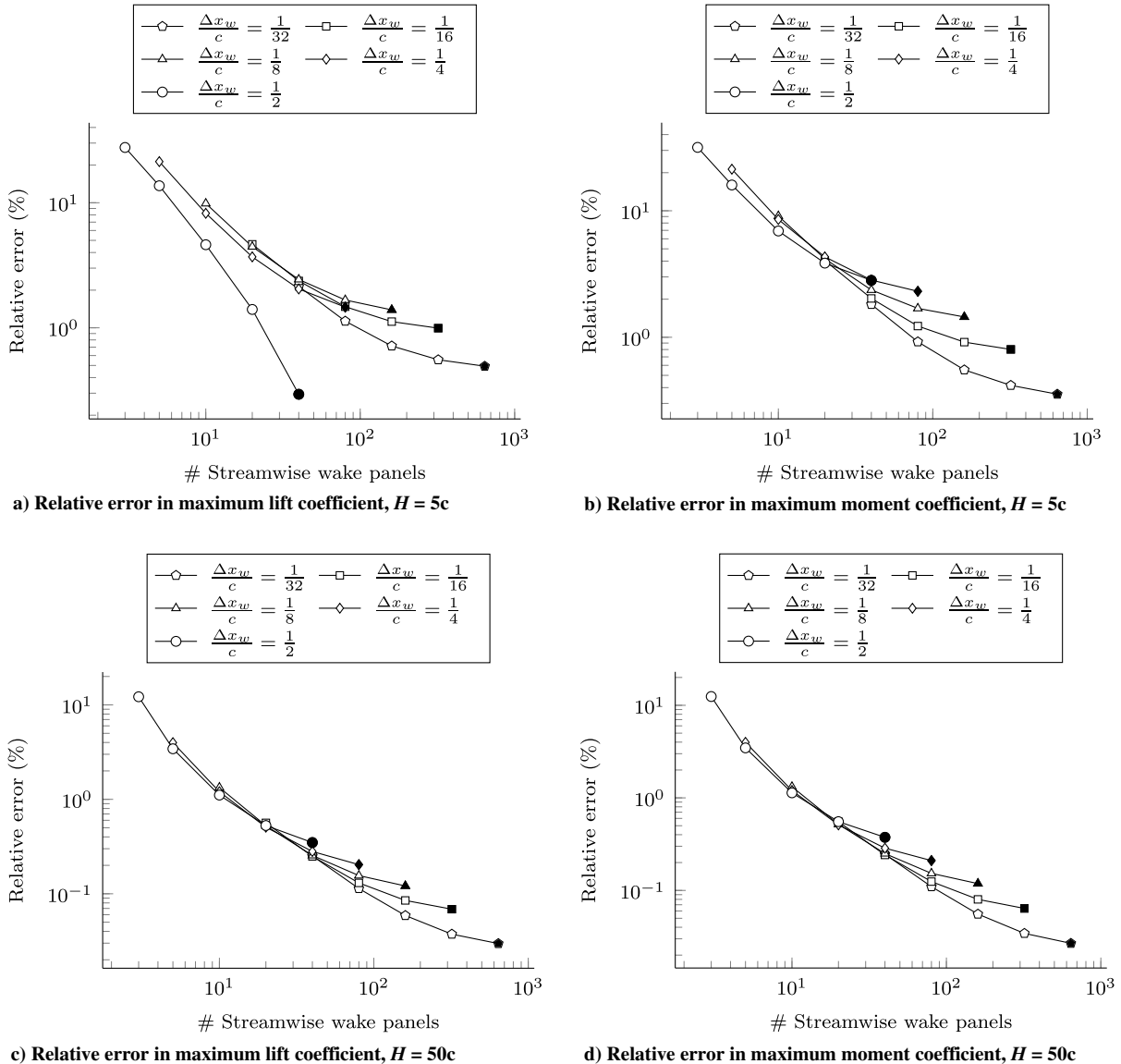


Fig. 9 Varying the number of streamwise wake panels for various initial wake panel sizes. Equivalent constant size wake discretization results are indicated by filled markers. The solution with a constant wake element size of $\Delta x_w/c = 1/64$ and corresponding time step of $V_\infty \Delta t/c = 1/64$ has been used as reference solution.

where A controls the ratio in size between two adjacent elements. The value of A can be determined by solving Eq. (35) for the first wake element based on the prescribed size of the first wake element $\Delta x_w/c$, which defines r , and the desired number of elements, which defines ρ .

The results indicate the advantage of a variable wake element size on the efficiency of computation. The main conclusion that can be drawn from these results is the tradeoff that can be made between model size and accuracy. For a small penalty in accuracy, the number of states in the system can be significantly reduced by reducing the number of wake panels. For example, for a gust length of 5 chords, the same accuracy can be achieved by a first wake element size of $\Delta x_w/c = 1/32$ and a wake with 80 streamwise wake panels as for a constant wake discretization of $\Delta x_w/c = 1/16$ and 320 streamwise wake panels, resulting in a reduction in the number of states by a factor of 4.

In conclusion, the present model allows for unsteady aerodynamic simulations with increased efficiency with respect to discrete-time and currently available continuous-time approaches by varying the wake element size and time step, thus reducing the required system size for a given accuracy. Furthermore, in case of gust simulations for aircraft, where many different load cases and gust lengths need to be run, a single efficient model can be set up, while computational efficiency is maintained by varying the time step size as required.

IV. Conclusions

A continuous-time state-space unsteady aerodynamic model has been presented for efficient load analysis of general aircraft wings. Based on potential flow theory, under a thin-wing assumption, vortex ring elements are used to set up the governing discretized equations for flow tangency and the Kutta condition. Using the advection equation to describe the transport of vorticity in the wake, under the assumption of small perturbations with respect to the steady solution and a fixed wake, the governing continuous-time state-space system has been derived by discretizing the advection equation only in space, while making no assumption for the time derivatives. The main advantage of the present approach is its flexibility, allowing for any arbitrary wake shape or discretization to be used and straightforward generalization to higher-order panel methods. The states of the system are the vortex strengths of the wake vortex elements and the perturbation angle of attack, and the input of the system is the time derivative of the perturbation angle of attack.

Verification of the present unsteady aerodynamic model with results in the literature shows excellent agreement. Comparison of the present model with the approximate closed-form solution by Lin and Iliff [42] to Possio's integral equation for the pressure distribution of a lifting surface in two-dimensional, oscillatory, subsonic compressible flow shows excellent agreement in amplitude up to a reduced frequency of one

across a range of Mach numbers, whereas for the phase angle, at a Mach number of 0.8 and a reduced frequency of one, the error is only 10 deg. The results thus show that the present model provides sufficiently accurate dynamic load predictions at low to moderate Mach numbers and reduced frequencies encountered in the normal operating conditions of aircraft. Note, however, that at Mach numbers above 0.7 care should be taken in applying both the present model and the closed-form solution, because, depending on the wing geometry, the underlying assumptions of the linearized potential flow equations might no longer be valid and, for example, solutions to the Euler equations or full potential equations might be necessary for accurate results.

Finally, the model has been applied to the gust analysis of a general swept and tapered wing, showing the benefits of the present approach by varying the time step and introducing a nonuniform wake discretization, resulting in a reduced model size for a given accuracy.

To investigate the benefits of the proposed approach in more detail, in future work, the method can, for example, be extended to prescribed wake geometries including the effects of, for example, steady wake roll up or to unstructured wake discretizations.

In conclusion, the resulting model can be used for the efficient loads analysis of general aircraft wings, including the effects of compressibility. Its continuous-time state-space implementation allows for any arbitrary wake shape to be modeled and easy integration with structural or flight dynamic models for efficient aero(servo)elastic analysis using a wake discretization and time step solely governed by accuracy requirements.

Appendix A: Derivation of the State Equation

As derived in Secs. II.C and II.D, the system of equations governing the potential flow solution around a wing is given by Eqs. (13), (16), and (28):

$$\begin{aligned} \mathbf{K}_1 \Gamma_b + \mathbf{K}_2 \Gamma_{w_0} + \mathbf{K}_3 \Gamma_w &= -\mathbf{V} \cdot \mathbf{n} \\ \mathbf{K}_4 \Gamma_b + \mathbf{K}_5 \Gamma_{w_0} &= \mathbf{0} \\ \mathbf{K}_6 \Gamma_w + \mathbf{K}_7 \Gamma_{w_0} &= \dot{\Gamma}_w \end{aligned}$$

with $-\mathbf{V} \cdot \mathbf{n}$ for a panel p defined by Eq. (15):

$$-\mathbf{V}_p \cdot \mathbf{n}_p = \underbrace{-V_\infty n_{x_p}}_{\text{mean steady flow}} + \underbrace{-V_\infty n_{z_p} \alpha}_{\text{freestream perturbation}} + \underbrace{-V_\infty \cdot \Delta \mathbf{n}_p + \mathbf{V}_b \cdot \mathbf{n}_p}_{\text{motion of the wing surface}}$$

Focusing on the unsteady aerodynamic solution around the mean steady flow, Eq. (13) can be written as

$$\mathbf{K}_1 \Gamma_b + \mathbf{K}_2 \Gamma_{w_0} + \mathbf{K}_3 \Gamma_w = \mathbf{B}_1 \alpha + \mathbf{B}_2 \quad (\text{A1})$$

where \mathbf{B}_1 represents the contribution of the freestream perturbation, and \mathbf{B}_2 represents the contribution of the motion of the wing surface.

Using Eq. (13), Γ_b can be written as function of Γ_{w_0} , Γ_w , the freestream perturbation, and the motion of the wing surface:

$$\Gamma_b = \mathbf{K}_1^{-1} (-\mathbf{K}_2 \Gamma_{w_0} - \mathbf{K}_3 \Gamma_w + \mathbf{B}_1 \alpha + \mathbf{B}_2) \quad (\text{A2})$$

When this is inserted in Eq. (16), Γ_{w_0} can be written as function of Γ_w , the freestream perturbation, and the motion of the wing surface:

$$\Gamma_{w_0} = (\mathbf{K}_5 - \mathbf{K}_4 \mathbf{K}_1^{-1} \mathbf{K}_2)^{-1} \mathbf{K}_4 \mathbf{K}_1^{-1} (\mathbf{K}_3 \Gamma_w - \mathbf{B}_1 \alpha - \mathbf{B}_2) \quad (\text{A3})$$

Substituting this relation in the wake transport equation, the state equation of the state-space system can be derived and the unsteady aerodynamic solution can be obtained:

$$\dot{\Gamma}_w = \mathbf{K}_8 \Gamma_w + \mathbf{K}_9 \alpha + \mathbf{K}_{10} \quad (\text{A4})$$

where

$$\mathbf{K}_8 = \mathbf{K}_6 + \mathbf{K}_7 (\mathbf{K}_5 - \mathbf{K}_4 \mathbf{K}_1^{-1} \mathbf{K}_2)^{-1} \mathbf{K}_4 \mathbf{K}_1^{-1} \mathbf{K}_3 \quad (\text{A5})$$

$$\mathbf{K}_9 = -\mathbf{K}_7 (\mathbf{K}_5 - \mathbf{K}_4 \mathbf{K}_1^{-1} \mathbf{K}_2)^{-1} \mathbf{K}_4 \mathbf{K}_1^{-1} \mathbf{B}_1 \quad (\text{A6})$$

$$\mathbf{K}_{10} = -\mathbf{K}_7 (\mathbf{K}_5 - \mathbf{K}_4 \mathbf{K}_1^{-1} \mathbf{K}_2)^{-1} \mathbf{K}_4 \mathbf{K}_1^{-1} \mathbf{B}_2 \quad (\text{A7})$$

Appendix B: Derivation of the Output Equation

Starting from Eq. (16) to write Γ_{w_0} as a function of Γ_b

$$\Gamma_{w_0} = -\mathbf{K}_5^{-1} \mathbf{K}_4 \Gamma_b \quad (\text{B1})$$

and introducing this in Eq. (13), the vortex strength of the body panels can be related to the vortex strength of the free wake panels Γ_w , the freestream perturbation, and the motion of the wing surface, resulting in

$$\Gamma_b = -\mathbf{L}_3^{-1} \mathbf{K}_1^{-1} \mathbf{K}_3 \Gamma_w + \mathbf{L}_3^{-1} \mathbf{K}_1^{-1} \mathbf{B}_1 \alpha + \mathbf{L}_3^{-1} \mathbf{K}_1^{-1} \mathbf{B}_2 \quad (\text{B2})$$

where $\mathbf{L}_3 = \mathbf{I} - \mathbf{K}_1^{-1} \mathbf{K}_2 \mathbf{K}_5^{-1} \mathbf{K}_4$ with \mathbf{I} as the identity matrix, \mathbf{B}_1 represents the contribution of the freestream perturbation, and \mathbf{B}_2 represents the contribution of the motion of the wing surface, similar to Appendix A. Taking the time derivative of this equation, grouping all terms related to the motion of the wing surface, and substituting this in Eq. (19), the following equation for the aerodynamic forces and moments is found:

$$\begin{bmatrix} \mathbf{F} \\ \mathbf{M} \end{bmatrix} = \mathbf{L}_4 \Gamma_w + \mathbf{L}_5 \alpha + \mathbf{L}_6 \dot{\Gamma}_w + \mathbf{L}_7 \dot{\alpha} + \mathbf{L}_8 \quad (\text{B3})$$

where

$$\mathbf{L}_4 = -\mathbf{L}_1 \mathbf{L}_3^{-1} \mathbf{K}_1^{-1} \mathbf{K}_3 \quad (\text{B4})$$

$$\mathbf{L}_5 = \mathbf{L}_1 \mathbf{L}_3^{-1} \mathbf{K}_1^{-1} \mathbf{B}_1 \quad (\text{B5})$$

$$\mathbf{L}_6 = -\mathbf{L}_2 \mathbf{L}_3^{-1} \mathbf{K}_1^{-1} \mathbf{K}_3 \quad (\text{B6})$$

$$\mathbf{L}_7 = \mathbf{L}_2 \mathbf{L}_3^{-1} \mathbf{K}_1^{-1} \mathbf{B}_1 \quad (\text{B7})$$

$$\mathbf{L}_8 = \mathbf{L}_1 \mathbf{L}_3^{-1} \mathbf{K}_1^{-1} \mathbf{B}_2 + \mathbf{L}_2 \mathbf{L}_3^{-1} \mathbf{K}_1^{-1} \dot{\mathbf{B}}_2 \quad (\text{B8})$$

Finally, using Eq. (A4), Eq. (B3) can be reduced to

$$\begin{bmatrix} \mathbf{F} \\ \mathbf{M} \end{bmatrix} = \mathbf{L}_9 \Gamma_w + \mathbf{L}_{10} \alpha + \mathbf{L}_7 \dot{\alpha} + \mathbf{L}_{11} \quad (\text{B9})$$

where $\mathbf{L}_9 = \mathbf{L}_4 + \mathbf{L}_6 \mathbf{K}_8$, $\mathbf{L}_{10} = \mathbf{L}_5 + \mathbf{L}_6 \mathbf{K}_9$, and $\mathbf{L}_{11} = \mathbf{L}_8 + \mathbf{L}_6 \mathbf{K}_{10}$.

References

- [1] Murua, J., Palacios, R., and Graham, J. M. R., "Applications of the Unsteady Vortex-Lattice Method in Aircraft Aeroelasticity and Flight Dynamics," *Progress in Aerospace Sciences*, Vol. 55, Nov. 2012, pp. 46–72. doi:10.1016/j.paerosci.2012.06.001
- [2] Thomas, J. P., Dowell, E. H., and Hall, K. C., "Nonlinear Inviscid Aerodynamic Effects on Transonic Divergence, Flutter, and Limit-Cycle Oscillations," *AIAA Journal*, Vol. 40, No. 4, 2002, pp. 638–646. doi:10.2514/2.1720
- [3] Thomas, J. P., Dowell, E. H., and Hall, K. C., "Modeling Viscous Transonic Limit Cycle Oscillation Behavior Using a Harmonic Balance Approach," *Journal of Aircraft*, Vol. 41, No. 6, 2004, pp. 1266–1274. doi:10.2514/1.9839
- [4] Beran, P. S., Khot, N. S., Eastep, F. E., Snyder, R. D., and Zweber, J. V., "Numerical Analysis of Store-Induced Limit-Cycle

- Oscillation," *Journal of Aircraft*, Vol. 41, No. 6, 2004, pp. 1315–1326.
doi:10.2514/1.404
- [5] Kholodar, D. B., Dowell, E. H., Thomas, J. P., and Hall, K. C., "Limit Cycle Oscillation of a Typical Airfoil in Transonic Flow," *Journal of Aircraft*, Vol. 41, No. 5, 2004, pp. 1067–1072.
doi:10.2514/1.618
- [6] Geuzaine, P., Brown, G., Harris, C., and Farhat, C., "Aeroelastic Dynamic Analysis of a Full F-16 Configuration for Various Flight Conditions," *AIAA Journal*, Vol. 41, No. 3, 2003, pp. 363–371.
doi:10.2514/2.1975
- [7] Farhat, C., "CFD-Based Nonlinear Computational Aeroelasticity," *Encyclopedia of Computational Mechanics*, Wiley, Hoboken, NJ, 2004, pp. 459–480.
- [8] Raveh, D. E., Levy, Y., and Karpel, M., "Efficient Aeroelastic Analysis Using Computational Unsteady Aerodynamics," *Journal of Aircraft*, Vol. 38, No. 3, 2001, pp. 547–556.
doi:10.2514/2.2795
- [9] Raveh, D. E., "CFD-Based Models of Aerodynamic Gust Response," *Journal of Aircraft*, Vol. 44, No. 3, 2007, pp. 888–897.
doi:10.2514/1.25498
- [10] Raveh, D. E., "Gust-Response Analysis of Free Elastic Aircraft in the Transonic Flight Regime," *Journal of Aircraft*, Vol. 48, No. 4, 2011, pp. 1204–1211.
doi:10.2514/1.C031224
- [11] Reimer, L., Ritter, M., Heinrich, R., and Krger, W., "CFD-Based Gust Load Analysis for a Free-Flying Flexible Passenger Aircraft in Comparison to a DLM-Based Approach," *22nd AIAA Computational Fluid Dynamics Conference*, AIAA Paper 2015-2455, 2015.
- [12] Iovnovich, M., and Raveh, D. E., "Reynolds-Averaged Navier-Stokes Study of the Shock-Buffer Instability Mechanism," *AIAA Journal*, Vol. 50, No. 4, 2012, pp. 880–890.
doi:10.2514/1.J051329
- [13] Raveh, D. E., and Dowell, E. H., "Aeroelastic Responses of Elastically Suspended Airfoil Systems in Transonic Buffeting Flows," *AIAA Journal*, Vol. 52, No. 5, 2014, pp. 926–934.
doi:10.2514/1.J052185
- [14] Patil, M. J., Hodges, D. H., and Cesnik, C. E. S., "Nonlinear Aeroelasticity and Flight Dynamics of High-Altitude Long-Endurance Aircraft," *Journal of Aircraft*, Vol. 38, No. 1, 2001, pp. 88–94.
doi:10.2514/2.2738
- [15] Patil, M. J., and Hodges, D. H., "On the Importance of Aerodynamic and Structural Geometrical Nonlinearities in Aeroelastic Behavior of High-Aspect-Ratio Wings," *Journal of Fluids and Structures*, Vol. 19, No. 7, 2004, pp. 905–915.
doi:10.1016/j.jfluidstructs.2004.04.012
- [16] Peters, D. A., Karunamoorthy, S., and Cao, W.-M., "Finite State Induced Flow Models. I—Two-Dimensional Thin Airfoil," *Journal of Aircraft*, Vol. 32, No. 2, 1995, pp. 313–322.
doi:10.2514/3.46718
- [17] Leishman, J. G., and Nguyen, K. Q., "State-Space Representation of Unsteady Airfoil Behavior," *AIAA Journal*, Vol. 28, No. 5, 1990, pp. 836–844.
doi:10.2514/3.25127
- [18] Albano, E., and Rodden, W. P., "A Doublet-Lattice Method for Calculating Lift Distributions on Oscillating Surfaces in Subsonic Flows," *AIAA Journal*, Vol. 7, No. 2, 1969, pp. 279–285.
doi:10.2514/3.5086
- [19] Roger, K., "Airplane Math Modelling and Active Aeroelastic Control Design," AGARD Technical Rept. CP-228, 1977.
- [20] Karpel, M., "Design for Active Flutter Suppression and Gust Alleviation Using State-Space Aeroelastic Modeling," *Journal of Aircraft*, Vol. 19, No. 3, 1982, pp. 221–227.
doi:10.2514/3.57379
- [21] Karpel, M., Moulin, B., and Chen, P. C., "Dynamic Response of Aeroservoelastic Systems to Gust Excitation," *Journal of Aircraft*, Vol. 42, No. 5, 2005, pp. 1264–1272.
doi:10.2514/1.6678
- [22] Kier, T. M., and Looye, G.-J. H., "Unifying Manoeuvre and Gust Loads Analysis Models," *International Forum on Aeroelasticity and Structural Dynamics*, Paper IFASD-2009-106, 2009.
- [23] Katz, J., and Plotkin, A., *Low-Speed Aerodynamics*, Cambridge Univ. Press, Cambridge, England, U.K., 2001, pp. 419–433.
- [24] Hall, K. C., "Eigenanalysis of Unsteady Flows about Airfoils, Cascades, and Wings," *AIAA Journal*, Vol. 32, No. 12, 1994, pp. 2426–2432.
doi:10.2514/3.12309
- [25] Murua, J., Palacios, R., and Graham, J. M. R., "Assessment of Wake-Tail Interference Effects on the Dynamics of Flexible Aircraft," *AIAA Journal*, Vol. 50, No. 7, 2012, pp. 1575–1585.
doi:10.2514/1.J051543
- [26] Stewart, E. C., Patil, M. J., Canfield, R. A., and Snyder, R. D., "Aeroelastic Shape Optimization of a Flapping Wing," *Journal of Aircraft*, Vol. 53, No. 3, 2016, pp. 636–650.
doi:10.2514/1.C033278
- [27] Mohammadi-Amin, M., Ghadiri, B., Abdalla, M. M., Haddadpour, H., and De Breuker, R., "Continuous-Time State-Space Unsteady Aerodynamic Modeling Based on Boundary Element Method," *Engineering Analysis with Boundary Elements*, Vol. 36, No. 5, 2012, pp. 789–798.
doi:10.1016/j.enganabound.2011.12.007
- [28] Morino, L., "Boundary Integral Equations in Aerodynamics," *Applied Mechanics Reviews*, Vol. 46, No. 8, 1993, pp. 445–466.
doi:10.1115/1.3120373
- [29] Blair, M., "A Compilation of the Mathematics Leading to the Doublet Lattice Method," Defense Technical Information Center WL-TR-92-3028, Fort Belvoir, VA, 1992.
- [30] Giesing, J. P., Kalman, T. P., and Rodden, W. P., "Subsonic Unsteady Aerodynamic for General Configurations Part I, Vol I—Direct Application of the Nonplanar Doublet-Lattice Method," U.S. Air Force Flight Dynamics Lab. TR-71-5, Wright-Patterson AFB, OH, 1971.
- [31] Drela, M., "Integrated Simulation Model for Preliminary Aerodynamic, Structural, and Control-Law Design of Aircraft," *40th Structures, Structural Dynamics, and Materials Conference and Exhibit*, AIAA Paper 1999-1394, 1999.
- [32] Simpson, R. J. S., Palacios, R., and Murua, J., "Induced-Drag Calculations in the Unsteady Vortex Lattice Method," *AIAA Journal*, Vol. 51, No. 7, 2013, pp. 1775–1779.
doi:10.2514/1.J052136
- [33] Reed, W. H., and Hill, T. R., "Triangular Mesh Methods for the Neutron Transport Equation," Los Alamos Scientific Lab., Technical Repts. LA-UR-73-479, CONF-730414-2, Los Alamos, NM, 1973.
- [34] Li, B. Q., *Discontinuous Finite Elements in Fluid Dynamics and Heat Transfer*, Computational Fluid and Solid Mechanics, Springer-Verlag, London, 2006, pp. 21–43, 157–180.
- [35] Hesse, H., and Palacios, R., "Reduced-Order Aeroelastic Models for Dynamics of Maneuvering Flexible Aircraft," *AIAA Journal*, Vol. 52, No. 8, 2014, pp. 1717–1732.
doi:10.2514/1.J052684
- [36] Voutsinas, S. G., "Vortex Methods in Aeronautics: How to Make Things Work," *International Journal of Computational Fluid Dynamics*, Vol. 20, No. 1, 2006, pp. 3–18.
doi:10.1080/10618560600566059
- [37] Willis, D. J., Peraire, J., and White, J. K., "A Combined pFFT-Multipole Tree Code, Unsteady Panel Method with Vortex Particle Wakes," *International Journal for Numerical Methods in Fluids*, Vol. 53, No. 8, 2007, pp. 1399–1422.
doi:10.1002/(ISSN)1097-0363
- [38] Theodorsen, T., "General Theory of Aerodynamic Instability and the Mechanism of Flutter," NACA TR 496, 1935.
- [39] Jones, W., "Aerodynamic Forces on Wings in Non-Uniform Motion," H.M. Stationery Office, Technical Rept. ARC-2117, London, 1945.
- [40] Katz, J., "Calculation of the Aerodynamic Forces on Automotive Lifting Surfaces," *Journal of Fluids Engineering*, Vol. 107, No. 4, 1985, pp. 438–443.
doi:10.1115/1.3242507
- [41] Wang, Z., Chen, P. C., Liu, D. D., and Mook, D. T., "Nonlinear-Aerodynamics/Nonlinear-Structure Interaction Methodology for a High-Altitude Long-Endurance Wing," *Journal of Aircraft*, Vol. 47, No. 2, 2010, pp. 556–566.
doi:10.2514/1.45694
- [42] Lin, J., and Iliff, K. W., "Aerodynamic Lift and Moment Calculations Using a Closed-Form Solution of the Possio Equation," NASA TM-2000-209019, 2000.
- [43] Weatherill, N., Soni, B., and Thompson, J., "Transfinite Interpolation (TFI) Generation Systems," *Handbook of Grid Generation*, edited by R. E. Smith, CRC Press, Boca Raton, FL, 1998, Chap. 3.
doi:10.1201/9781420050349.ch3